

**The interpretation of multi-frequency acoustic profiling: Part 1. Exact solutions and their role in the evaluation of acoustic backscatter models.****David R. Topham**

ASL Environmental Sciences Inc., Saanichton, BC, Canada

**Correspondence:** David R. Topham ([dtopham@aslenv.com](mailto:dtopham@aslenv.com))**Abstract**

A set of multi-frequency acoustic equations, sufficient to describe a suspension in terms of a two parameter distribution function defined with  $n$  equivalent volume sphere, is examined to determine the conditions necessary to provide valid solutions for a given data set. For three incident acoustic frequencies, the equations are fully determined, and in principle, exact solutions exist. A criterion is established to determine the existence of exact 3-frequency solutions directly from the data before undertaking analysis. With access to four or more frequencies, comparisons of alternative independent 3-frequency solutions provide a measure of the quality of the match between backscatter model and data, providing a powerful diagnostic tool. The methodology is illustrated by examples drawn from an elastic sphere backscatter model, with a frazil ice data set providing an example of evaluation where the particle geometry differs maximally from the elastic sphere model.

**1. Introduction**

The use of near simultaneous sequences of high frequency acoustic pulses to establish the physical properties of populations of suspended matter is a long established technique in many fields, including sediment transport and ocean biomass studies. In most cases, the extraction of physical properties of the target from backscattered acoustic energy is well understood, and is backed by an extensive body of literature (Hay and Sheng, 1992; Crawford and Hay, 1993; Stanton et al. 1997). However, more recent applications of the technique to formation of frazil ice in rivers, (Marko and Jasek, 2010, Marko et al. 2015, Marko and Topham, 2021, McFarlane et al. 2017), and in the vicinity of Antarctic ice shelves (Frazer et al. 2020, Kungl et al. 2020), are less well developed, with questions arising as to the acoustic scattering properties of disk-shaped ice particles.

Here, a set of acoustic equations is examined to determine conditions for an acoustic backscatter model to provide valid solutions for multi-frequency data returned by suspension. Specifically, volume backscatter coefficients measured at each of  $n$  frequencies are matched to corresponding model values, providing a set of  $n$  equations. Where the number of free parameters in the model is equal to the number of acoustic frequencies, the equations are fully determined and the solutions are computationally exact. Practical applications are commonly described by a 2-parameter,

lognormally distributed particle suspension: Crawford and Hay (1993) for sediment transport, or for frazil ice, Clark and Doering, (2006), McFarlane et al., (2017?), where three frequencies suffice to define a fully determined set of acoustic equations. The determination of the accuracy of the predicted physical properties of the target requires additional acoustic frequencies. These generate a set of independent, high precision solutions, each representing the same physical target: their inter-comparison then provides a measure of the match between the theoretical model and the data set. The differences are absolute, in the sense that they reflect inherent properties of the model and the data, independent of the convergence of the algorithm. In cases where confidence in the model is high, the comparison provides error estimates for the physical properties of the acoustic target. Conversely, with good data, the comparison serves to evaluate the model.

## 2.0 Basic theory of measurements and extraction procedures.

The analysis is subject to the following assumptions:

1. That the total flux of backscattered acoustic energy is the sum of the energy scattered by individual particles.
2. That the normalized particle backscatter cross section,  $\sigma_{BS}/\pi\hat{a}^2$  is a unique function of the parameter  $k_I\hat{a}$ , where  $k_I$  is the incident acoustic wavenumber, and  $\hat{a}$  a characteristic acoustic length scale of an individual particle.

The length scale  $\hat{a}$  is defined here as  $a_e$ , the “effective radius” of an equal volume sphere, (Ashton, 1983), reflecting the inherent dependence of the physical scattering on target volume. This optimizes the solutions for estimates of suspended fractional volume.

Data is specified in terms of volume backscatter coefficients,  $s_V(\nu_i)$ , defined as the fraction of acoustic power incident on a unit volume suspension at a frequency  $\nu_i$ , which is scattered directly back towards its source. In general terms, the backscattered energy balance for measurements made in each of  $n$  different frequency channels can be expressed as:

$$s_V(\nu_i) = N \int_0^{\infty} g(a_e) \sigma_{BS}(a_e, \nu_i) da_e \quad , \quad (1)$$

where  $N$  is the total number of particles per unit volume, and  $\sigma_{BS}(a_e, \nu_i)$  the theoretical backscatter cross section of an individual particle at an acoustic frequency  $\nu_i$ . The latter is distributed according to a two parameter probability distribution,  $g(a_e)$ , satisfying:

$$\int_0^{\infty} g(a_e) da_e = 1 \quad . \quad (2)$$

For present purposes,  $g(a_e)$  is taken as the 2-parameter lognormal distribution:

$$g(a_e, a_m, b) = [(2\pi)^{0.5} b a_e]^{-1} e^{-0.5 \left( \frac{\ln(a_e/a_m)}{b} \right)^2} \quad , \quad (3)$$

where the descriptive population parameters  $a_m$ , and  $b$ , are the mean effective radius and the standard deviation. The set of equations in  $N$ ,  $a_m$ , and  $b$  is then fully determined for three frequencies.

The particle number density  $N$  appears as a common multiplying factor, and is eliminated by division to express the equations in terms of ratios of backscatter coefficients (Hay and Sheng, 1992). The ratios are denoted by  $G(i,j)$ , where the indices  $i$  and  $j$  identify the individual data channels, ie.  $G(2,1)^{meas} \equiv s_V(v_2)/s_V(v_1)$ , etc. This step produces a new set of  $n!/(2(n-2)!)^2$  equations (i.e. equal the number of possible combinations of  $(n-1)$  frequency pairs) of the form:

$$G(i,j)^{meas} = G(i,j) , \quad (4)$$

where the unscripted symbol  $G(i,j)$  denotes the functional relationship defined by the ratio of the right hand member of the set of equations (1), the superscripted symbols  $G(i,j)^{meas}$  are the corresponding  $s_V$  data ratios. In the case of the 2-parameter distribution adopted here, the equations reduce to a pair of ratios sharing a common frequency, in principle providing a computationally exact solution for the distribution parameters  $a_m$  and  $b$ . The number density  $N$  and fractional volume  $F$  then follows from the measured  $s_V(v_i)$  values via equations (1) and (5), for the fully determined equations, are independent of the choice of frequency.

Corresponding estimates of fractional volume  $F$  are given by,

$$F = N \int_0^\infty \left(\frac{4\pi}{3}\right) g(a_e, a_m, b) a_e^3 da_e . \quad (5)$$

The solution of the particle distribution parameters is obtained from a simple least squares routine, defined by the vanishingly small value of the residual  $Q$ :

$$Q = \sum_1^m [G(i,j)^{meas} - G(i,j)]^2 \quad (6)$$

where  $m$  is the number of frequency pairs. Differences in the values of  $N$  returned by individual frequencies provide an interpretation of the residual  $Q$  in terms of physical parameters of the suspension.

Considering just two frequencies reduces the problem to the less informative, but more widely applicable, two-channel analysis previously used by Marko and Jasek (2010). This limits the characterization of suspensions to the reduced parameters  $a^*$  and  $N^*$ , representing the target as a suspension of uniformly sized particles. The set of equations (4) then reduces to a single equation in  $a^*$  for each of the independent  $G(i,j)^{meas}$  ratios, where the volume backscatter coefficient equation simplifies to

$$s_V(v_i) = N^* \sigma_{BS}(a^*, v_i), \quad (7)$$

While this representation does not realistically describe the details of the target suspension, the inherent dependence of the physical scattering on target volume produces relatively robust estimates of the fractional volume parameter  $F^*$ , where:

$$F^* = \frac{4\pi}{3} N^* a^{*3} . \quad (8)$$

For a suitably narrow particle distribution,  $F^*$  is a good approximation to  $F$ .

## 2.1 The characteristics of the exact solutions.

The general structure of the solutions for the set of ratio equations (4), is discussed in a graphical framework, illustrated by the example of the elastic sphere, (Faran, 1951) and complemented by data drawn from the 2011-12 Peace River 4-frequency frazil ice deployment of Marko et al. (2015). Data were acquired at, 125 kHz, 235 kHz, 455 kHz and 774 kHz respectively. Erratic behaviour of the 235 kHz channel 2 data, limited examples to the three channels 1, 3, and 4, providing access to three, independent 2-channel solutions, and one 3-channel solution. For discussion purposes, the normalized backscatter cross section for an elastic sphere of ice suspended in fresh water is shown in Fig 1: the circular symbols refer to the analysis of frazil ice data in Section 3.

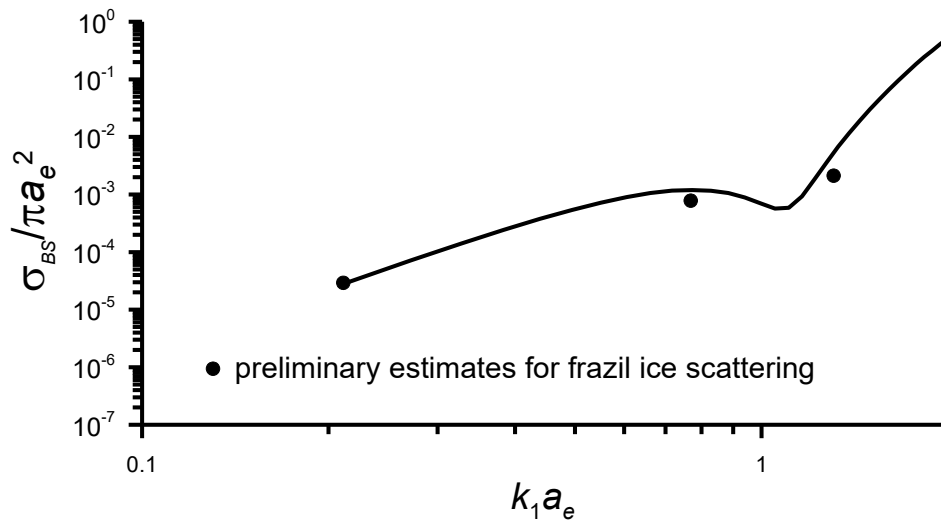


Figure 1. The normalized backscatter cross section for an elastic sphere of ice suspended in freshwater. Symbols indicate possible modifications deduced from data analysis as described in Section 3.

### 2.1.1 Two-channel solutions.

Each channel pair ratio provides an independent description of the physical parameters of the target. Solutions are determined by the intersections of the data, represented by the horizontal lines, with the corresponding theoretical functions  $G(i,j)$ , Fig. 2. The data examples are drawn from the Peace River data of Table 2, Section 3.

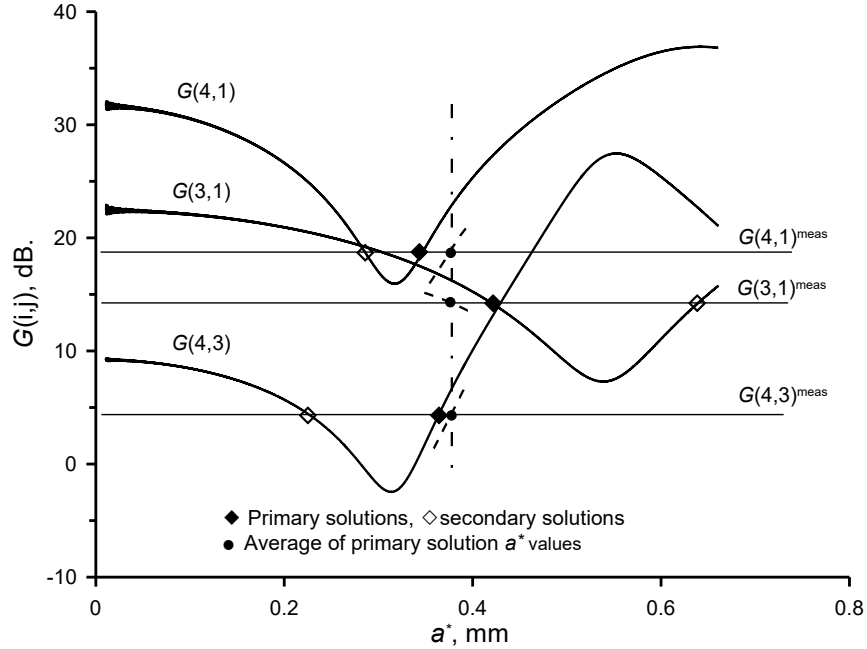
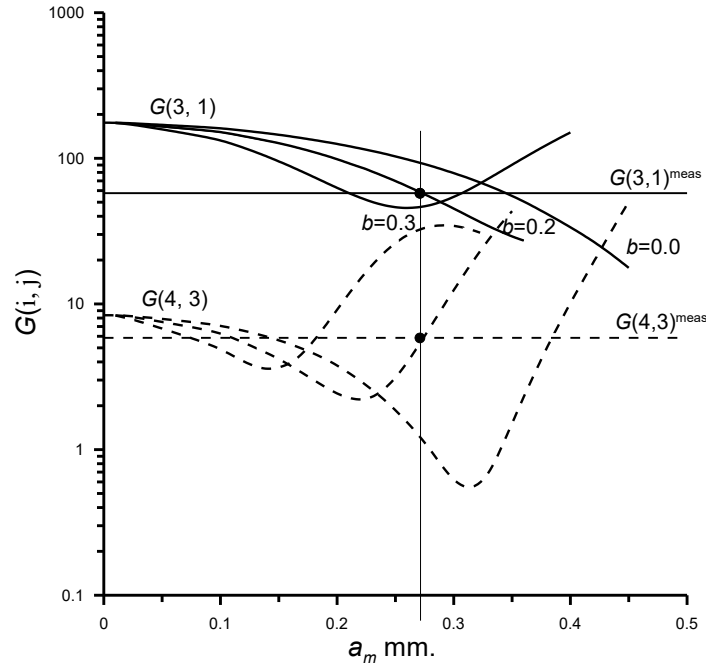


Figure 2. Illustration of two-frequency solutions obtained from intersections, denoted by diamond-shaped markers, of measured (4,1), (3,1) and (4,3) backscatter coefficient ratios (light horizontal lines) with corresponding theoretical functions. The vertical broken line marks the mean value of  $a^*$  of 0.38 mm. The displaced dashed segments of the curves relate to the discussion of Section 3.

The  $G(i,j)$  functions are two-valued within the range of interest, with solutions marked by diamond symbols, and designated as “lower” and “upper” branch solutions with respect their respective minima. The physically relevant solutions for the three channel combinations, marked by solid diamonds, represent the same physical target, and their dispersion about the mean value, marked by the chain dotted line, is a measure of the overall accuracy. The secondary solutions, marked by open symbols, are more widely dispersed, and, in this example, are easily distinguished. For solutions occurring close to the  $G(i,j)$  minima, the correct choice of solution can be problematic, and is resolved by consideration of the three-channel solutions.

### 2.1.2 Three channel solutions

For the exact, fully determined, three-channel solutions, two  $G(i,j)$  functions sharing a common frequency must be solved simultaneously. The structure of the solutions is illustrated in Fig. 3 for a family of the (3,1) and (4,3) channel combinations as full and dashed lines respectively, each pair identified by the particle distribution parameter  $b$ . The horizontal lines represent input ratios for a hypothetical input data point with the solution  $a_m = 0.274$  mm, and  $b=0.2$ , (marked by the symbols). Note that the second intersection of the data with the lower branch of the  $G(4,3)$  function has no matching  $G(3,1)$  intersection, establishing that the three-channel solutions are single valued, and confined to the upper branch of the  $G(4,3)$  curve.



**Figure 3.** A graphical illustration of a three-channel solution using the (3,1) and (4,3) channel pairs. The solution space is specific to the elastic sphere model.

In the limit as  $b$  approaches zero, the branch pairings define the branch of corresponding two-channel solutions for each included channel pair, resolving the previously noted two-channel ambiguity. The branch pairings of the  $G(i,j)$  functions for the possible three-channel combinations are listed in Table 1. Each pairing contains the same frequency information, and represents the same solution. The solution branches are unique to the individual channel pairs and hence define the relevant branches of the corresponding two-channel solutions.

Branch pair combinations	
$G(4,1)$ Upper	$G(4,3)$ Upper
$G(3,1)$ Lower	$G(4,3)$ Upper
$G(3,1)$ Lower	$G(4,1)$ Upper

Table 1. Branch pair combinations for the 3-channel elastic sphere solutions.

Each value of  $a_m$  defines a pair of boundary points on Fig. 3 enclosing a range of input data capable of supporting three-channel solutions; the upper and lower boundaries are defined by the  $G(3,1)_{b=0}$  and  $G(4,3)_{b=0}$  curves respectively, (corresponding boundaries can be defined for the alternative channel pairings listed in Table 1). The relationship between corresponding boundary values establishes the necessary condition for the data to support solutions. Solutions for particular values of  $b$  are further constrained to  $a_m$  values between the minimum of the  $G(4,3)$  function and its intersection with the  $G(3,1)$  function. Where the functions fail to intersect, as illustrated for  $b = 0.3$ , solutions are limited by the minimum of the  $G(3,1)$  function. These criteria enable the existence and particle distribution width of the exact solutions to be established directly from a data set before undertaking a full analysis.

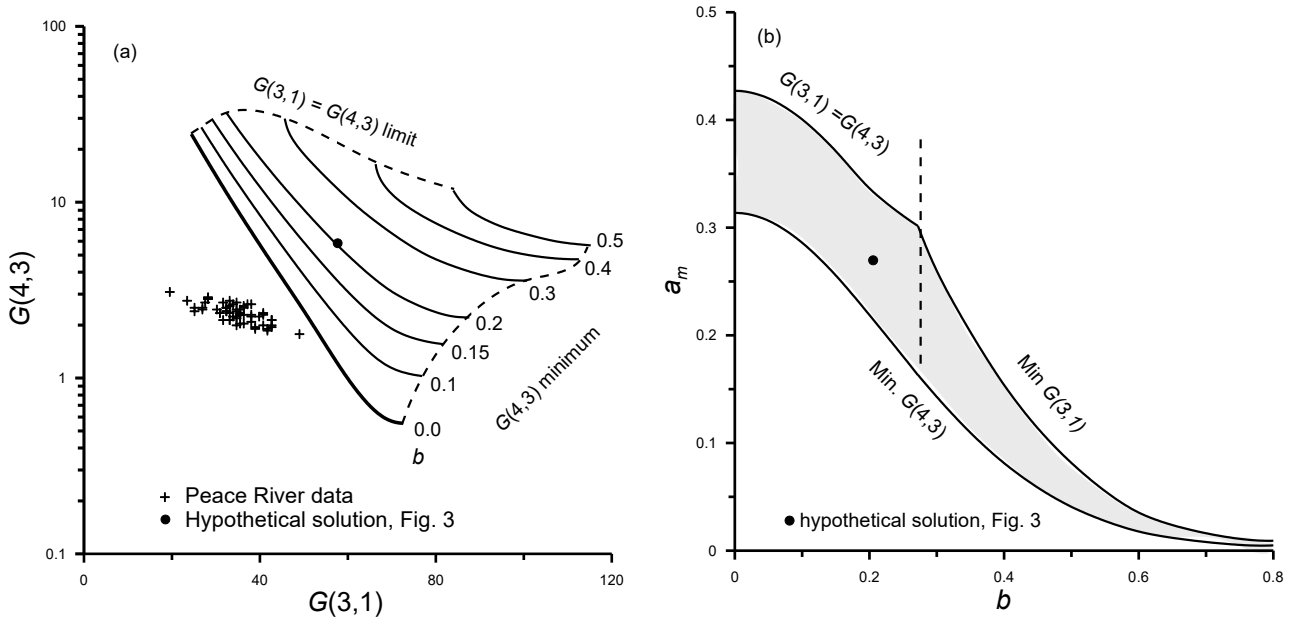


Figure 4. (a) The existence diagram for elastic sphere 3-frequency solutions, + data points for Peace River frazil ice; (b) The solution map for the elastic sphere.

Fig. 4a shows the full existence diagram for 3-channel solutions of the elastic sphere  $G(3,1)$  and  $G(4,3)$  pairing, the thicker line indicating the critical  $b = 0$  boundary. The data points indicate of the absence of 3-channel solutions for the March 20 Peace River frazil interval. Figure 4b maps the corresponding parameter boundaries in  $(b, a_m)$  space. In cases where solutions exist, appropriate initial values of  $a_m$  and  $b$  must be assigned to ensure convergence. Ideally, these should be within the shaded area of Fig 4b, the value of  $b$  being available from Fig. 4a. For the elastic sphere case illustrated here, initial conditions below the lower boundary of Fig. 4b also converge. When 3-channel solutions are sought in the absence of the exact solutions, the search algorithm progresses to  $b \approx 0$ , with a value of  $a_m$  approximating the mean of the three possible individual 2-channel solutions. Differences between the physical parameters derived from each frequency, then provide an estimate of their uncertainty.

### 3.0 Evaluation of the elastic sphere as a backscatter model for disk shaped frazil ice.

The four frequency data set provides a total of six, 2-frequency, and four, 3-frequency independent, fully determined solutions for a three parameter backscatter model. The standard deviation of the 2-frequency solutions then provides a robust measure of the uncertainty of output parameters, with individual differences highlighting specific ranges of the backscatter cross section relationship. The final solution is then taken as the mean of the 3-frequency solutions, conditioned by the standard deviation of the 2-frequency solutions.

The availability of a set of multi-frequency frazil ice data of suspensions provided the opportunity to evaluate the elastic sphere as a backscatter model for a weakly buoyant suspension of disk

shaped particles. The analysis was carried out on 2-minute averaged Peace River  $s_V$  data from the 20 March, 2012 frazil interval (Marko et al., 2015). The 3-frequency existence criterion established that no exact solutions are found for the elastic sphere analysis, Fig. 4a. Likewise, a times series of the existence of 2-frequency solutions, Fig. 5, revealed the poor quality of the channel two data.

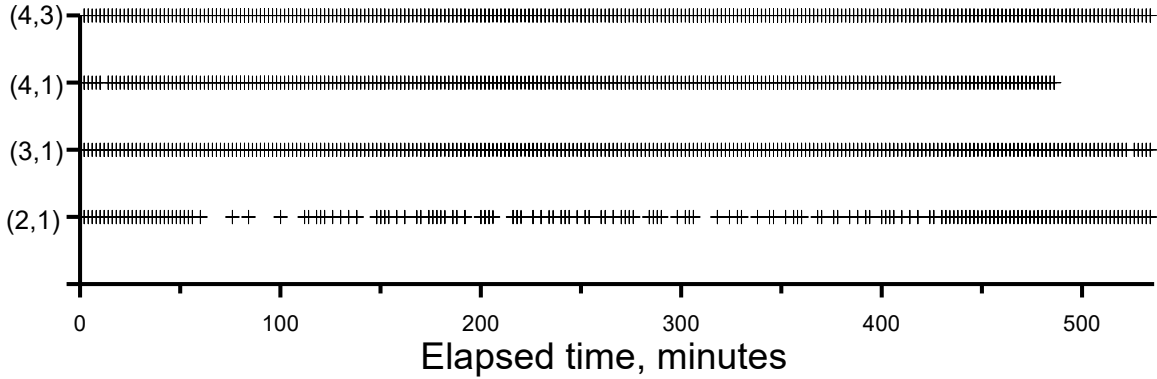
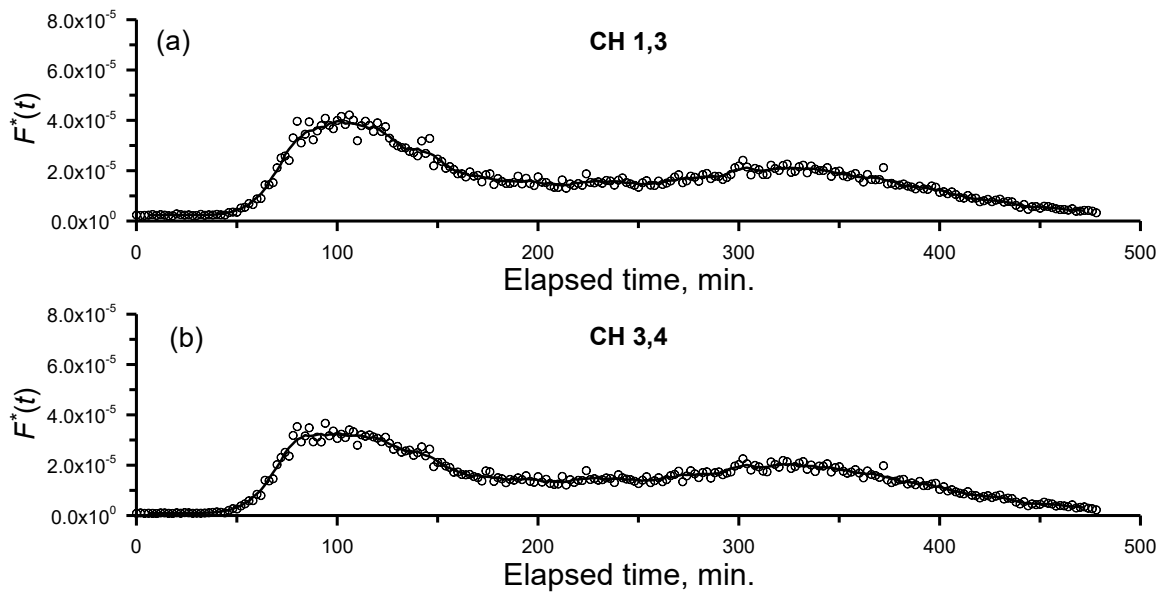


Figure 5. Time series indicating the existence of the 2-frequency solutions.

The evaluation, therefore, is confined to 2-frequency analysis of the channel pairs (3,1), (4,1) and (4,3) under the assumption of a uniform particle distribution. Figures 6a, b and c, respectively provide an overview of the full time series of  $F^*$  for the three channel pairings. Panels (a) and (b) are similar, with somewhat lower peak values for the latter case. Panel (c), the case where the channel pair is separated by the full range of available frequencies, has a more prominent peak, and overall, a notably exaggerated scatter.



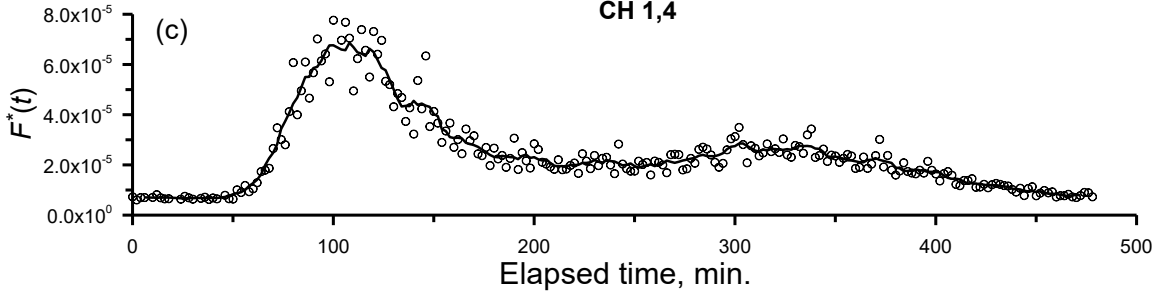


Figure 6. Comparisons of the March 20 frazil fractional volume as derived with the data channel combinations: (a), (3,1); (b), (4,1) and (c), (4,3).

Detailed quantitative comparisons focus on the 90-110 minute interval encompassing the peak fractional volumes. Key results and relevant parameters deduced for this period are summarized in the first three rows of Table 2 for the available channel pairings. Listed values are overall averages of two-channel extractions from ten individual data points and are equivalent to a single time averaged data set centred on the peak of the curves of Fig.6.

Channels	Peak $a_e^*$	Peak $F^*(t)$	Peak $N^*(t)$	$F^*(t)/F^*_{Mean}$	Lowest value of $k_{1a_e^*}$ or $k_{1a_m}$	Highest value of $k_{1a_e^*}$ or $k_{1a_m}$
3,1 (lower)	0.420	$3.85 \times 10^{-5}$	$1.24 \times 10^5$	0.847	0.235	0.856
4,3 (upper)	0.365	$3.15 \times 10^{-5}$	$1.55 \times 10^5$	0.694	0.744	1.265
4,1 (upper)	0.346	$6.63 \times 10^{-5}$	$3.82 \times 10^5$	1.46	0.194	1.200
Mean	0.377	$4.54 \times 10^{-5}$	$2.20 \times 10^5$	1	-	-

**Table 2.** Two-channel frazil fractional volume extractions from  $s_V$  data.

The entries in the first column specify pair composition and the relevant branch of the corresponding  $G(i,j)$  curve. The final two columns list values of  $k_{1a_e}$  corresponding to the lowest and highest acoustic frequency associated with each extraction. The opposing effects of changes in  $a_e^*$  and  $N^*$  allow relatively robust estimates of fractional volume,  $F^*$ , reflecting the dominant role of target volume in the scattering response of the weakly buoyant suspensions. The  $F^*$  values for the (3,1) and (4,3) channel pairs differ by 20%, an encouraging result, given that the joint  $k_{1a_e}$  range embraces the local minimum of the sphere cross section relationship. For the (4,1) pair, spanning the upper and lower  $k_{1a_e}$  extremes, the  $F^*$  value exceeds the (3,1) and (4,3) pair values by a factor of roughly 2, giving the final estimate of the mean  $F^*$  as  $4.54 \times 10^{-5} \pm 1.8 \times 10^{-5}$ .

The mismatch between the model and data is illustrated graphically in Fig. 2, where the offset dotted line segments indicate the changes in the model  $s_V$  ratios required to match the input values. Assuming that  $k_{1a_e}$  values associated with channel 1 data are sufficiently low for modified backscatter relationship to be represented by the elastic sphere model, the downward shifts in the  $G(i,j)$  functions translate into corresponding shifts in the normalized cross section relationship, indicated by the solid points on Figure 1. These suggested modifications are consistent with laboratory measurements on polystyrene disks and spheres, Marko and Topham, (2015).

## 4.0 Summary and conclusions

The necessary conditions are examined for a theoretical acoustic model to deliver valid solutions for a given multi-frequency acoustic backscatter data set. A fundamental requirement is that the theoretical backscatter cross section  $\sigma$  be a unique function of a characteristic length scale of the acoustic target particle. Since the primary interest is in the fractional volume of suspended material, the characteristic length scale is defined in terms of the “effective radius”  $a_e$ , ie. that of a sphere of volume equal to acoustic target. This reflects the dominant role of target volume in the scattering response of the weakly buoyant suspensions. Note that the backscatter cross section relationship  $\sigma(k/a_e)$  is a general function, not necessarily that of the sphere. The theoretical model features a 2-parameter particle distribution, and for three acoustic frequencies the set of equations is fully determined, and in principle solutions are computationally exact.

To realise the exact solutions, the equations are expressed in terms of ratios of the equated backscatter quantities. For pairs of ratios sharing a common frequency (i.e. a frequency triplet), these equations provide exact solutions for the particle distribution parameters  $a_m$  and  $b$ . The particle number density  $N$  is calculated independently from the measured  $s_v$  values. A relationship between the two theoretical backscatter ratios establishes the existence conditions for corresponding data ratios to support fully determined 3-frequency solutions. The existence of exact solutions can thus be established directly from a data set prior to full analysis.

As used here, the term “exact” refers to the precision of algorithmic solution, not to the derived physical properties of the target suspension. This requires measurements at additional frequencies to provide alternative, independent, solutions; their inter-comparison then provides a measure of the quality of the match between the backscatter model and data. The validation procedure is greatly enhanced by the inclusion of the 2-frequency solutions, the number of ratios increasing factorially with the number of frequencies. For example, a 4-frequency data set supplies six, independent 2-frequency solutions, and four, independent 3-frequency solutions. The 2-frequency solutions return information from a specific regions of the backscatter relationship, providing a powerful diagnostic tool. The high precision of the solutions allows a backscatter model to be calibrated directly to field data, a valuable asset in cases where realistic conditions are difficult to reproduce in the laboratory. Conversely, for a well calibrated model, the evaluation acts as a pre-analysis filter to locate inappropriate data points.

The general methodology is illustrated throughout by results obtained using the Faran (1951) theory of scattering by elastic spheres, coupled with a established lognormal particle distribution. Evaluation procedures are demonstrated by application of the sphere theory to a typical Peace River frazil ice data set, wherein the thin disk geometry of the targets deviates maximally from the spherical geometry assumed by the model. The existence criterion establishes that while the elastic sphere model cannot provide 3-frequency solutions, the less restrictive 2-frequency analysis provides frazil fractional volumes to about 60% uncertainty, and suggests possible modifications of the Faran spherical backscatter model sufficient to satisfy the 3-frequency existence criteria. These modifications, included in Fig 1, are consistent with laboratory measurements on polystyrene disks and spheres (Marko and Topham, 2015) and have motivated subsequent

successor work (Topham and Marko, 2023b) directed at developing and evaluating a semi-empirical frazil cross section relationship.

## References

- Ashton, G. D., 1983: Frazil ice. In: Theory of Dispersed Multiphase Flow, Academic Press N.Y., 271-289.
- Clark, S., Doering, J. 2006: Laboratory Experiments on Frazil Size Characterizations in a Counterrotating Flume, J. Hydraulic Engineering, pp, 94-101.
- Crawford, A. M. and Hay, A. E., 1993: Determining suspended sand size and concentration from multifrequency acoustic backscatter. J. Acoust. Soc. Am. 94 (6) pp. 3312-3324.
- Faran, J.J. Jr., 1951: Sound scattering by solid cylinders and spheres. J. Acoust. Soc. 23, pp 405-418.
- Frazer, E. K., Langhorne, P. J, Leonard, G. H., Robinson, N.J. and Dániel Schumayer, D. Observations of the size distribution of frazil ice in an ice shelf water plume., 2020. Geophys. Res. Letters, 47, e2020GL090498, <https://doi.org/10.1029/2020GL090498>.
- Hay, A. E, and Sheng, J. 1992: Vertical profiles of suspended sand concentrations and size from multifrequency acoustic backscatter. J. Geophys. Res. 97 (10), pp 1566-1567.
- Kungl, A. F., Schumayer, D., Eamon K. Frazer, A. K., Pat J. Langhorn, P. J., Greg, H., Leonard, G. H., 2020: An oblate spheroidal model for multi-frequency acoustic back-scattering of frazil ice. Cold Reg. Sci Technol, 177, <https://doi.org/10.1016/103122>.
- Marko, J.R., Jasek, M., 2010: Frazil monitoring by multi-frequency shallow water ice profiling (SWIPSA): present state. Proc. IAHR 20<sup>th</sup> International Symposium on Ice, Lahti, Finland. 12p.
- Marko, J.R., Jasek, M., Topham, D.R., 2015: Multifrequency Analyses of 2011-2012 Peace River SWIPS frazil backscattering data. Cold Reg. Sci. Technol. 110, 102-119.
- Marko, J. R. & Topham, D.R. (2015). Laboratory measurements of acoustic backscattering from polystyrene pseudo- ice particles as a basis for quantitative frazil characterization. Cold Reg. Sci. Technol. 112, 66-86. <https://doi.org/10.1016/j.coldregions.2015.01.003>

Marko, J.R., Topham, D.R., 2021: Analyses of Peace River shallow water ice profiling sonar data and their implications for the roles played by frazil ice and in situ anchor ice growth in a freezing river. *The Cryosphere* 15, 2473-2489, [https://doi. Org/10.5194/tc-13-2473](https://doi.org/10.5194/tc-13-2473).

McFarlane, V., Loewen, M., Hicks, F., 2017: Measurements of the size distributions of frazil ice particles in three Alberta rivers. *Cold Reg. Sci. Technol.* 142, pp. 100-117,

Stanton, T.K, Wiebe, P.H., Chu, D., 1998: Differences between sound scattering by weakly scattering spheres and finite-length cylinders with applications to sound scattering by zooplankton. *J. Acoust. Soc. Am.* 103 (1).